Numerical simulation and experimental investigation on the residual stresses in a laser beam welded dual phase DP600 steel plate: Thermo-mechanical material plasticity model

S. Liu, A. Kouadri-Henni, A. Gavrus

Numerical simulation and experimental investigation on the residual stresses in a laser beam welded dual phase DP600 steel plate: thermo-mechanical material plasticity model

S. LIU, A. KOUADRI-HENNI*, A. GAVRUS

Université Bretagne Loire (UBL), France

INSA Rennes-LGCGM-EA 3913, 20 avenue des Buttes de Coësmes, 35708,Rennes, France

Abstract

A thermo-mechanical plasticity material model, which consists of a hardening and a temperature sensitivity term, is built to describe the dual phase DP600 steel behavior. For the hardening term, a synthesis Ludwik - Voce hardening law is proposed, identified and compared with the classical Ludwik and the Voce hardening laws. For the temperature sensitivity function, a new proposed expression together with a classical Johnson-Cook term and an improved Chen term are analyzed and identified. Moreover, the plate anisotropy of DP600 is also taken into account using Hill-48 theory. Based on the plasticity material model, a numerical sequential coupled thermo-mechanical model is applied to investigate the residual stresses of laser welding process. It is shown that the material anisotropy and the thermo-mechanical elastic-plastic model have an important influence on numerical residual stresses results. An experiment is also carried out to verify the numerical model. Simulation results of residual stresses are in good accordance with neutrons diffraction measurements.

Keywords: Constitutive Equations, Anisotropy, Laser Welding, DP600 Dual Phase Steel Behavior, Residual Stress, Neutron Diffraction

*email address: afia.kouadri-henni@insa-rennes.fr

1. Introduction

In the aim of reducing energy consumption and CO_2 release, high strength alloy is widely used to reduce the car weight in automotive industries (Davies (2012)). Among the high strength low weight alloys, the dual-phase (DP) steel possesses adequate ductility and high strength. DP600 contains about 15% hard martensite in a soft ferrite matrix (Calcagnotto et al. (2011); Marya and Gayden (2005)). The body-centered-tetragonal martensite helps to improve the high strength while the body-centered-cubic ferrite contributes to ductility (Chen et al. (1989); Kuang et al. (2009)). DP600 has no-yield-point elongation and a higher strain-hardening rate than traditional high-strength low-alloy (HSLA) steels (Fekete and Stibich (2001)). The high strain-hardening rate can increase absorption energy in car collision, thus helps to decrease damage (Bouaziz et al. (2013)).

Nd:YAG laser welding is an efficient way in car manufacture. With appropriate welding parameters, the process can produce a firm joint. But welding may also change material property and introduce potential safety and reliability issues. When laser welding is used on dual-phase (DP) materials, the influence of material property should be investigated, such as the microstructure, tensile strength, hardness and fatigue properties by N. Farabi et al (Farabi et al. (2011)), mechanical and metallurgical properties by M. Hazratine et al (Hazratinezhad et al. (2012)) and the formability by M. Xia et al (Xia et al. (2008)). To better evaluate the performance of DP600 welding joint, the residual stresses are investigated in this paper both numerically and experimentally.

In simulation domain, the strain hardening phenomenon can be modeled by defining the material plasticity. Among various mathematical expressions, Ludwik equation (Ludwik (1909)) and Voce equation (Voce (1955)) are two widely used constitutive models for material plasticity. As plastic strain increases, the flow stress increases in Ludwik model, while reaches a constant value in Voce model. Ludwik constitutive model is suitable for martensite hardening phenomenon, while Voce model for ferrite. Since DP600 is a combination of martensite and ferrite, a synthesis constitutive equation is used to describe the material plasticity. Besides the hardening, a temperature sensitivity term is proposed and compared with Johnson-Cook model (John and Cook (1983)) and Chen model (Chen et al. (2008)) for plasticity model.

Along different directions, DP600 sheet presents different plastic behavior. The anisotropy of DP600 sheets is usually a result of large deformation during

rolling operations in manufacturing. To describe anisotropy of material, a number of theory can be applied to material, such as Hill-48 (Hill (1948)), Srp93 (Barlat and Chung (1993)) and Yld-2004-18p (Barlat et al. (2005)). Among these theories, Hill-48 theory is one of the most famous theories which describes the material's anisotropy with six parameters F, G, H, L, M, N. The values for DP600 have been reported by works (Padmanabhan et al. (2007); Rabahallah et al. (2009); Ozturk et al. (2014)), which reveal that the anisotropy in rolled sheet influences subsequent material behavior and affects the strain distributions.

To ensure weld performance, residual stresses of DP600 lap welding joint is investigated. A thermo-mechanical finite element model (FEM) is built through commercial code ABAQUS. The hardening behavior and temperature sensitivity of DP600 are considered in the model through UHARD subroutine. The anisotropy of DP600 are considered in the simulation model and the result suggest that different material rolling orientations influence numerical simulation of residual stresses obviously. Simulation results of residual stresses are compared with the experimental measurements of neutron diffraction technique, and good accordances are found.

2. Numerical model

A laser beam of 4kW power and 3.4m/min welding speed was used to weld two plates of dual phase DP600 steel. Concerning the elastic properties of the DP600 dual phase steel the numerical simulations uses the following generic values: Young's modulus E = 210GPa, Poison's ratio $\nu = 0.28$ and thermal expansion coefficient $\alpha = 1.2 \times 10^{-5}\mathrm{K}^{-1}$. The detail description about thermal analysis, elastic and expansion behaviors of laser welding DP600 steel can be referred to a previous work (Seang et al. (2013)). This paper focus on the thermo-plasticity material model. The residual stresses analysis uses a sequential coupled thermo-mechanical analysis. The simulation model consists of two parts:

1. Thermal analysis part
    - Heat source, heat transfer and boundary condition of radiation and convection are considered to analysis the thermal data using an ABAQUS model
2. Mechanical analysis part

- A predefined field is used to introduce thermal analysis results so that the previous calculated thermal data is used as an input data file for a mechanical analysis of residual stress distribution.
- With the consideration of material property, such as the expansion behavior of the material due to temperature increase, the elastic and plastic behavior of the material, and the relaxation of the stresses at the cooling step, laser welding residual stresses are simulated.

In figure 1, the geometry, mesh and boundary condition of the mechanical model are presented. The path transversal to weld line, the rolling direction and the directions of residual stresses are illustrated. The angle between transversal path and rolling direction is θ. There are 44160 elements in total for the model and element type C3D8R is selected for analysis.

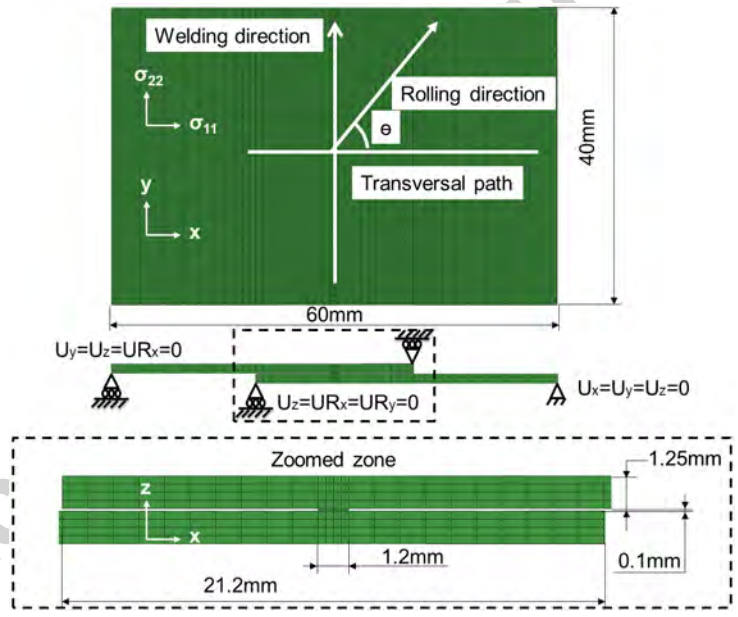

Figure 1: Mesh and geometry of numerical model

According to the material rheological behavior, the hardening influence, the softening phenomena, the strain rate sensitivity and the anisotropy influence of a dual phase DP600 steel are discussed. As proposed by Gavrus (Gavrus (2012)), based on theory of dislocations glides and mixture microstructures formulations proposed by Avrami, the plastic flow stress corre-

sponding to numerical simulation of dynamic forming process can be expressed in a general form as:

$$\sigma(\varepsilon_{\mathrm{p}}) = [\sigma_{\mathrm{h}}(\varepsilon_{\mathrm{p}}) \cdot (1-\psi) + \sigma_{\mathrm{s}} \cdot \psi] \cdot \mathrm{F}(T) \cdot G(\dot{\bar{\varepsilon}}) \tag{1}$$

where ε_p is the cumulated plastic strain, T is the temperature and $\dot{\bar{\varepsilon}}$ is the plastic strain rate. In this equation, $\sigma_h(\varepsilon_p)$ represents the hardening component, σ_s the saturation term and ψ the material fraction undergoing dynamic softening phenomena (dynamic recrystallization, phase transformation, twinning ...) or a dynamic recovery. F(T) is the temperature sensitivity, and $\mathrm{G}(\dot{\bar{\varepsilon}})$ is the strain rate sensitivity function. In a first approximation, during the laser welding simulation, the strain rate sensitivity can be chosen to be equal to unity i.e. $\mathrm{G}(\dot{\bar{\varepsilon}}) = 1$.

3. Hardening behavior

Table 1 presents all the rheological parameters of DP600 identified for different hardening models. The mathematical form of the hardening models are discussed in the following parts.

Table 1: Rheological coefficients corresponding to different DP600 hardening models

	σ_y	n_1	n_2	n_3	n_4	w	Equation	Nonlinear regression ε_p range
Classical Ludwik model 01	400	980	0.48	-	-	-	(2)	[0, 0.2]
Classical Ludwik model 02	400	1660	0.63	-	-	-	(2)	[0, 0.05]
Modified Ludwik model	400	1690	0.5	-1240	-65	-	(3)	[0, 0.2]
Classical Voce model 01	400	555	15.5	-	-	-	(4)	[0, 0.2]
Classical Voce model 02	400	340	27.5	-	-	-	(4)	[0, 0.05]
Modified Voce model	400	270	30	900	-	-	(5)	[0, 0.2]
Proposed synthesis model	400	1660	0.63	340	27.5	0.40	(6)	[0, 0.2]

3.1. Ludwik model

The initial yield stress marked as "σ_y" is the elastic limit after which the material starts its hardening. For a material phase such as the martensite one, the material flow stress $\sigma(\varepsilon_p)$ can be expressed by the Ludwik hardening model using a classical power form:

$$\sigma(\varepsilon_{\mathrm{p}}) = \sigma_{\mathrm{y}} + \mathrm{n}_1 \varepsilon_{\mathrm{p}}^{\mathrm{n}_2} \tag{2}$$

Ludwik model can be interpreted as a particular term of the general constitutive equation (1) defined by $[\sigma_h(\varepsilon_p) \cdot (1-\psi) + \sigma_s \cdot \psi]$ using the hardening stress expressed by $\sigma_h(\varepsilon_p) = \sigma_y + n_1 \varepsilon_p^{n_2}$ and a softening material fraction equal to 0 i.e. $\psi = 0$.

For the DP600 steel, the Ludwik model cannot fully fit the original experimental curve, so a mathematically modified form of Ludwik model is proposed to represent the observed material behavior:

$$\sigma(\varepsilon_{\mathrm{p}}) = \sigma_{\mathrm{y}} + \mathrm{n}_1 \varepsilon_{\mathrm{p}}^{\mathrm{n}_2} + \mathrm{n}_3 \varepsilon_{\mathrm{p}} + \mathrm{n}_4 \tag{3}$$

As can be seen in figure 2, "Classical Ludwik model 01" correspond to the classical form (equation 2) and "Modified Ludwik model" becomes a mathematical improvement of the Ludwik one. It is important to note that the addition of the linear term "$n_3\varepsilon_p + n_4$" in Equation 3 permits to fit more accurately the experimental data but has not any physical meaning. The straight line is used to obtain more accuracy of the obtained non-linear regression curve.

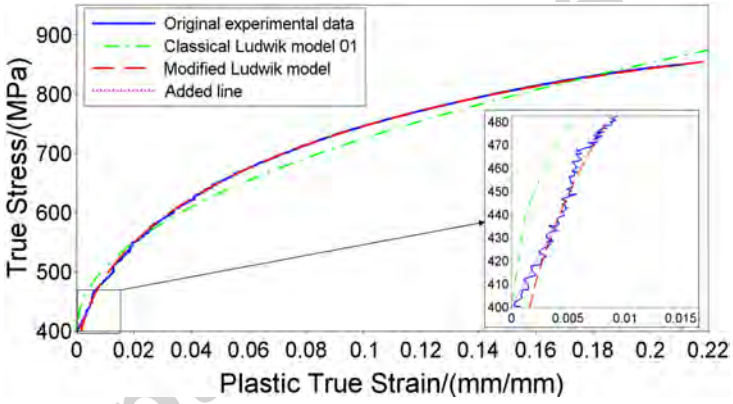

Figure 2: Comparison of Ludwik model and experimental DP600 data

3.2. Voce model

The Voce law is a good rheological formulation used to describe the material recovery (hardening with saturation plateaus) such as the plastic flow of the ferrite. The Voce model can be expressed in the following form (Voce (1955)):

$$\sigma(\varepsilon_{\mathrm{p}}) = \sigma_{\mathrm{y}} + \mathrm{n}_1 \cdot [1 - \exp(-\mathrm{n}_2 \varepsilon_{\mathrm{p}})] \tag{4}$$

In Equation 4, $\mathrm{n}_1 + \sigma_{\mathrm{y}}$ is the saturation stress and σ_y is the initial yield stress. Voce model can be interpreted in term of the general constitutive equation (1) where the term $[\sigma_h(\varepsilon_p) \cdot (1-\psi) + \sigma_s \cdot \psi]$ is written by the sum of $(n_1 + \sigma_y) \cdot [1 - exp(-n_2\varepsilon_p)]$ and $\sigma_y \cdot exp(-n_2\varepsilon_p)$ defining the hardening

term by $\sigma_h = n_1 + \sigma_y$, the saturation of plateaus term by $\sigma_s = \sigma_y$ and the recovery fraction by $\psi = exp(-n_2\varepsilon_p)$.

For the DP600 material, the plastic flow stress can not be perfectly fitted by the Voce equation, so a mathematically modified form is written below in order to fit the experimental curve.

$$\sigma(\varepsilon_p) = \sigma_{\mathrm{y}} + \mathrm{n}_1 \cdot [1 - \exp(-\mathrm{n}_2\varepsilon_{\mathrm{p}})] + \mathrm{n}_3\varepsilon_{\mathrm{p}} \tag{5}$$

As is seen in figure 3, "Classical Voce model 01" is the original form of Voce law and "Modified Voce model" is the mathematical improvement form of the classical Voce equation. The addition of the linear term "$n_3\varepsilon_p$" in Eqn. 5 only let the Voce equation to obtain a best fit of the original experimental data. This mathematical improvement is not based on the physical mechanisms characterizing the material plasticity and of the real mechanical behavior of hardness martensite / softening ferrite mixture, but can be regarded as a first approximation if an equal repartition of two phases is considered.

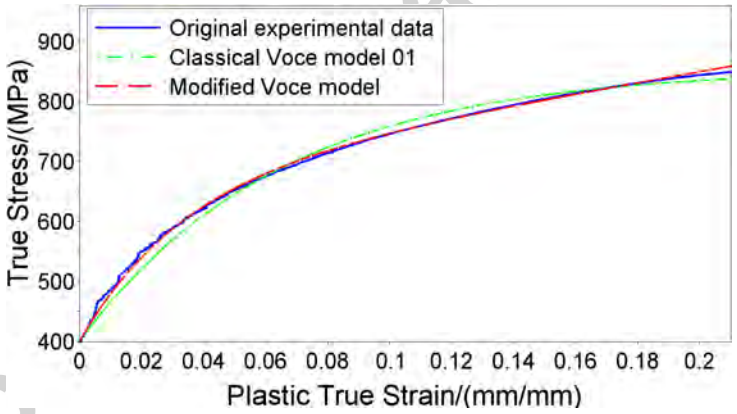

Figure 3: Comparison of Voce model and experimental DP600 data

3.3. Proposed synthesis model

According to the above considerations, mathematical improvements only for classical hardening laws to fit more accurately the experimental data are generally not physically based on material microstructure or plastic phenomena. Since DP600 is a dual phase material containing both martensitic and ferritic phases, a proper and physical rheological hardening model should

be defined. So based on equation (1), neglecting any phase transformation or dynamic softening phenomena (i.e. $\psi = 0$), using a hardening term σ_h defined by a mixture Avrami formulation available for static recovery phenomenon with a classical Ludwik model describing the ferritic recovery, and introducing the material fraction w to define the content of martensitic phase, a synthesis model is proposed by authors to define the hardening function $\sigma(\varepsilon_p)$ in the following form:

$$\begin{aligned}\sigma(\varepsilon_p) = w \cdot (\sigma_y + n_1 \varepsilon_p^{n_2}) \\ + (1-w) \cdot \{\sigma_y + n_3 \cdot [1 - exp(-n_4 \varepsilon_p)]\}\end{aligned} \tag{6}$$

The martensitic material fraction w can vary from 0 to 1. In this paper, w takes a value of 0.4 for the studied DP600 steel.

The figure 4 plot the difference between the experimental data, the classical Ludwik model and the classical Voce one (identified in the plastic strain range [0, 0.05]) and the proposed synthesis model (identified in the plastic strain range of all experimental results i.e. [0, 0.2]). It can be seen the advantage of the proposed synthesis model to obtain a very good agreement with all experimental measurements describing the real elasto-plastic behavior of dual phase DP600 steel, both for plastic strain range [0, 0.05] and [0.05, 0.2] corresponding to more localized deformations which can occur during the forming process.

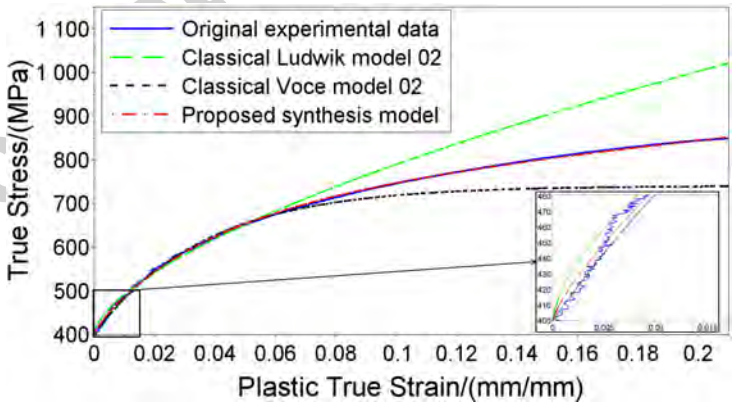

Figure 4: Comparisons of rheological models and experimental DP600 data

3.4. Residual stresses obtained from different hardening models

In figure 5, all the three models of figure 4 and the two modified models of figure 2 and figure 3 are input into FEM of ABAQUS by user subroutines as material models. For all five models, a Johnson-Cook temperature sensitivity term F(T) (John and Cook (1983)) is used and the conditions "F(298K)=1 and F(1803K)=0.05" is fulfilled with a mathematical value m = 0.104.

The simulation results of residual stresses along welding transversal path are shown.

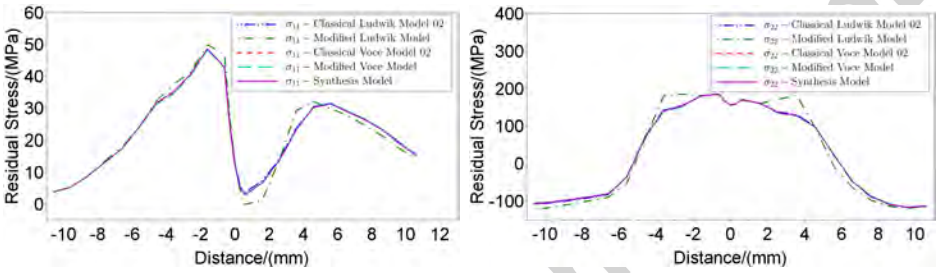

(a) Residual stresses of welding transversal direction

(b) Residual stresses of welding longitudinal direction

Figure 5: Residual stresses of different hardening models along transversal path

During this laser welding simulation, the maximum strain is no larger than 0.05, thus the five material hardening models are nearly the same within the range of $0 < \varepsilon_p < 0.05$, except for the "modified Ludwik" model where a straight line is added as is seen in figure 2. From the numerical simulation results analysis, one may conclude that as long as the stress-strain curves expressed by the material behavior models are similar within used small strain range, the forms of hardening equations have little influence on the numerical residual stresses estimation. However, the proposed synthesis rheological model describe precisely the experimental hardening material behavior of DP600 dual phase steel simultaneously for small and more important plastic strain values, it is already validated concerning numerical simulation of residual stresses corresponding to a laser welding process and can be used to analysis the process taking into account other initial operating conditions.

The contours of residual stresses σ_{11} and σ_{22} computed with the five hardening models are nearly the same and only results of the synthesis model is shown in the figure 6. The residual stresses at the plate surface are plotted

with contour curves. There are tensile stresses at the center zone of weld line and compressive stresses adjacent to weld line. The magnitude of residual stresses are not precise because the use of basic parameters for a classical Johnson-Cook temperature sensitivity formulation. To improve simulation results, several temperature sensitivity models are discussed in the following part.

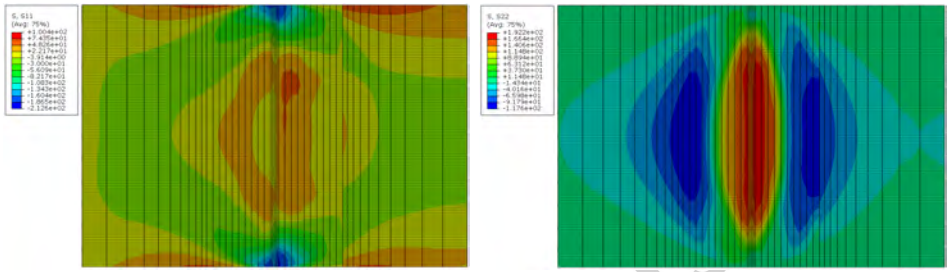

(a) Contour of residual stress σ_{11} of transversal direction

(b) Contour of residual stress σ_{22} of longitudinal direction

Figure 6: Simulation results of synthesis hardening model with a Johnson-Cook temperature sensitivity model

4. Temperature sensitivity

When a material is subjected to a high temperature, its strength tends to drop. In laser welding process, this phenomenon has a great effect on evaluation of elasto-plastic material behavior. In order to built a fine welding model and obtain good results of residual stresses, a proper material model taking into account the temperature sensitivity is investigated. Several temperature sensitivity models are taken into account and used to analysis the welding process. A lot of scientific works define the temperature sensitivity term $\mathrm{F}(T)$ in function of the homologous temperature T^*. Generally the homologous temperature T^* can be defined as:

$$T^* = \frac{T - \mathrm{T_r}}{\mathrm{T_{melt}} - \mathrm{T_r}} \tag{7}$$

$\mathrm{T_{melt}}$, T, $\mathrm{T_r}$ are melting, current, and room temperature, respectively. For DP600 steel, $\mathrm{T_{melt}}$ is supposed to be 1803.15 K and the room temperature is 298.15 K.

4.1. Arrhenius model

The temperature sensitivity of Arrhenius term (Samantaray et al. (2010)) is expressed by:

$$\mathrm{F}(T) = exp\left(\frac{\mathrm{m'Q}}{\mathrm{R}\,T}\right) \tag{8}$$

Where R is the universal gas constant, m′ is an adjustable parameter and Q the activation energy. Majority of thermo-mechanical plasticity applications consider a simplified expression using the thermal parameter $\beta = m'Q/R$.

4.2. Hirt model

Similar to Arrhenius model, the Hirt model is defined as:

$$\mathrm{F}(T) = exp\,(-\beta' T) \tag{9}$$

4.3. Linear model

The linear model can be viewed as an one order Taylor development of the exponential Hirt model:

$$\mathrm{F}(T) = exp\,(-\beta' T) = 1 - \beta' T + \cdots \tag{10}$$

Using "m" for "β'" and "$\mathrm{T} - \mathrm{T_r}$" to instead of "T" and avoid the rest, a simple linear model can be obtained.

The linear term of temperature sensitivity has been proposed by Hutchison (Hutchison (1963)) in 1960s. The material drops linearly with temperature increment.

$$\mathrm{F(T)} = 1 - \mathrm{m} \cdot (\mathrm{T} - \mathrm{T_r}) \tag{11}$$

Where m is a material coefficient and T_r is reference temperature. The linear model is simple in form but not suitable for rapid material strength drop.

4.4. Johnson-Cook model

About twenty years later, based on many experimental tests and phenomenological analysis, Johnson-Cook (John and Cook (1983)) proposed a well-founded material model which is still widely used nowadays to describe dynamic forming process. The temperature sensitivity term of Johnson-Cook model can well predict the material temperature sensitivity below about $\frac{1}{2}T_m$ but not well above. For Johnson-Cook model, T_r is room temperature to define T^* in Equation 7.

$$\mathrm{F}(T) = 1 - T^{*\mathrm{m}} \tag{12}$$

4.5. Khan model

A power function with respect to temperature T is proposed by Khan (Khan et al. (2004)) as a temperature sensitivity model. For Khan model, T_r is reference temperature, so Khan temperature sensitivity model can use different parameters "m" with different temperature range. The use of different parameters enable the model to predict material temperature sensitivity at high temperature range.

$$\mathrm{F}(T) = \left(\frac{\mathrm{T_m} - T}{\mathrm{T_m} - \mathrm{T_r}}\right)^m \tag{13}$$

4.6. Chen model

The Chen model (Chen et al. (2008)) contains the temperature sensitivity term as the following form. The Taylor development of the Chen model is "$1 + n \cdot T^{*\mathrm{m}} + \cdots$", so when "n" is set to "-1" and the Chen model can be viewed as a first order approximation of Johnson-Cook model.

$$\mathrm{F}(T) = exp(n \cdot T^{*\mathrm{m}}) \tag{14}$$

4.7. Proposed model

The proposed model can be viewed as a more general form equation as Johnson-Cook temperature model ($k = n = 1$).

$$\mathrm{F}(T) = (1 - \mathrm{k} \cdot T^{*\mathrm{m}})^{\mathrm{n}} \tag{15}$$

All the parameters of temperature sensitivity terms analyzed above are shown in Table 2. The parameters of the Chen model and the proposed model are identified by a non-linear least squares regression method.

Table 2: Parameters describing of temperature sensitivity

	m	n	k
Johnson-Cook	1.5	-	-
Khan model	0.5	-	-
Chen model	-28.418	4.254	-
Proposed model	4.207	38.629	0.699

The temperature sensitivity of the DP600 steel is supposed to be the same of the high strength steel in the work of Chen (Chen et al. (2006)). The

thermal softening fraction is the ratio of the stress at elevated temperature to that at room temperature. As is seen in figure 7, the thermal soften fraction is presented with different temperature sensitivity models by setting $\mathrm{F}(T_{room}) = 1$. The Johnson-Cook model and the Khan model can be suitable from room temperature to about 800 K, but not appropriate above 800 K. The Chen model and the proposed model are near to experiment data except for the data around 1000 K. A polynomial expression is used to precisely describe the experimental data.

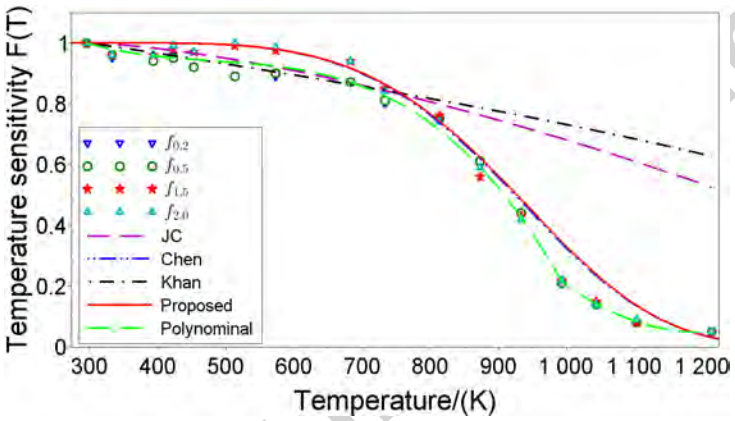

Figure 7: Temperature dependence of experiment data and simulation models

Because the proposed physical model, the Chen model and the mathematical polynomial model better fit the experimental data than the Johnson-Cook formulation and the Khan model for DP600 steel temperature sensitivity in welding simulation, thus only the first three models are employed into ABAQUS/FEM by UHARD subroutine. Simulation results of residual stresses along transversal path to weld are presented in the figure 8. Differences of residual stresses between the Chen model and the proposed one are found, though the two models are nearly the same in description of temperature sensitivity. Compared with the mathematical polynomial model (the best description of experimental temperature sensitivity), the proposed formulation leads to better residual stresses of transversal direction while the Chen model leads to better residual stresses of longitudinal direction.

In figure 9, the contours of residual stresses σ_{11} and σ_{22} simulated with Chen model, proposed model and polynomial model are presented. The values ranges of the legend are set the same for σ_{11} and σ_{22} respectively. The comparison shows some differences between the three models for residual

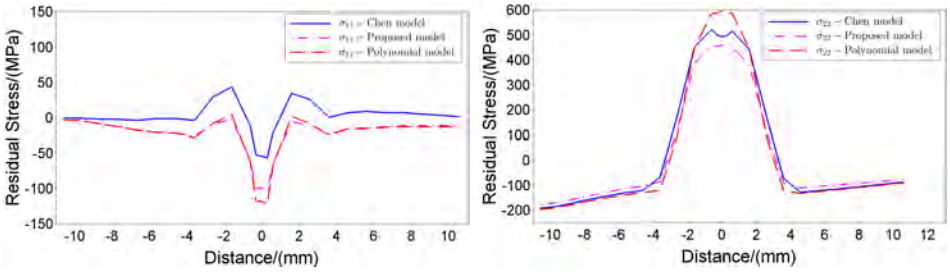

(a) Residual stresses of transversal direction

(b) Residual stresses of longitudinal direction

Figure 8: Influence of temperature sensitivity models

stresses distribution of σ_{11} and σ_{22} corresponding to the material behavior point of view where the thermal sensitivity term has an important influence.

5. Planar anisotropy

For nearly all plate materials, the rolling process would leave an anisotropy property. The anisotropy of DP600 steel is considered as planar anisotropy with Hill-48 theory. The Hill's potential function is an extension of the Mises function, which can be expressed in terms of rectangular Cartesian stress components as (Hibbitt et al. (1997)):

$$\begin{aligned} f(\sigma) = \big[&\mathrm{F}(\sigma_{22}-\sigma_{33})^2 + \mathrm{G}(\sigma_{33}-\sigma_{11})^2 \\ &+ \mathrm{H}(\sigma_{11}-\sigma_{22})^2 + 2\mathrm{L}\sigma_{23}^2 \\ &+ 2\mathrm{M}\sigma_{31}^2 + 2\mathrm{N}\sigma_{12}^2\big]^{1/2} \end{aligned} \tag{16}$$

where F, G, H, L, M, and N are the Hill coefficients obtained by tests of the material in different orientations. The effective stress $f(\sigma)$ is a scalar that dependent on material stress state and is a key value defining the plastic flow. Generally it is assumed to estimate this effective stress from the equivalent stress corresponding to the plastic flow curve obtained by tensile tests along the rolling direction. The specimen geometry used for tensile tests is shown in figure 10. The planar anisotropy is estimated using Hill-48 theory and the parameters are estimated according to the computation method presented in the work of Ohashi (Ohashi et al. (2012)).

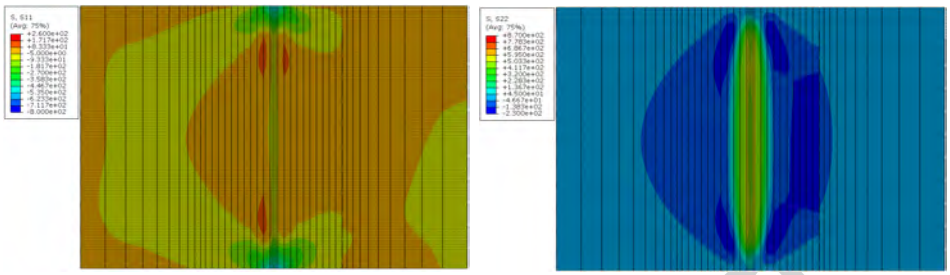

(a) σ_{11} of the Chen model (b) σ_{22} of the Chen model

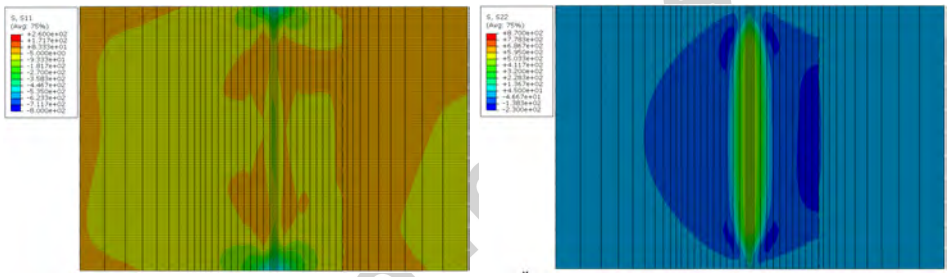

(c) σ_{11} of the Proposed model (d) σ_{22} of the Proposed model

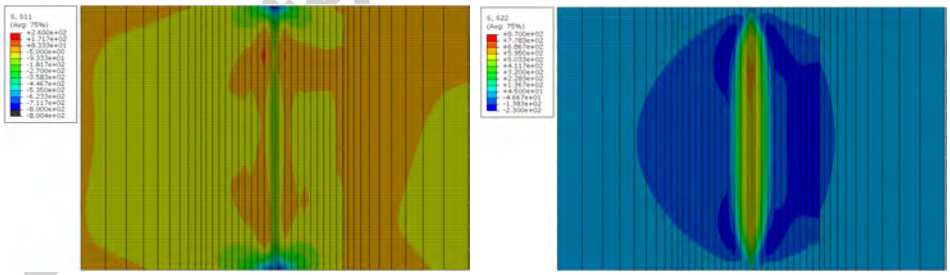

(e) σ_{11} of the Polynomial model (f) σ_{22} of the Polynomial model

Figure 9: Contour of residual stresses with different temperature sensitivity

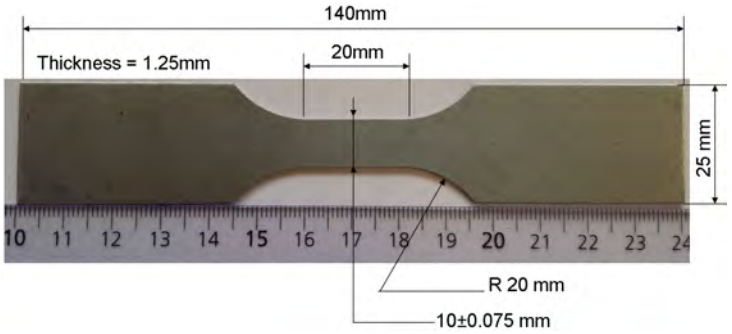

Figure 10: Dimensions of specimen for tensile test

Specimen are prepared so that the angle between the stretch direction and the rolling direction of DP600 are $\theta = 0°$, $\theta = 45°$ and $\theta = 90°$, respectively. At the beginning, the length and width of test area are noted as l_0 and w_0, respectively. The tensile test are conducted with a strain rate of $10^{-2}s^{-1}$. When the total strain $\varepsilon_{total} = 0.15$, specimen are unloaded and the length l_1 and width w_1 are measured. Along the three specimen directions, the corresponding measurements are presented in Table 3.

Table 3: Measurement of dimension change of tensile test

	$\theta = 0°$	$\theta = 45°$	$\theta = 90°$
Initial length l_0/mm	19.70	19.62	19.58
Unload length l_1/mm	21.18	21.30	21.04
Initial width w_0/mm	10.06	10.06	10.06
Unload width w_1/mm	9.70	9.74	9.72

The Lankford coefficient r (also known as width/thickness strain ratio) can be computed by

$$r = \frac{ln(w_1/w_0)}{ln(w_1 \cdot l_1/w_0 \cdot l_0)} \tag{17}$$

Specimens with different angles $\theta = 0°$, $\theta = 45°$ and $\theta = 90°$ are analyzed by tensile tests. The corresponding anisotropic coefficients are noted as r_0, r_{45} and r_{90} respectively.

Based on the r-values, the Hill parameters can be estimated from following formula:

$$F = \frac{r_0}{(1+r_0)r_{90}} \tag{18}$$

$$G = \frac{1}{1+r_0} \tag{19}$$

$$H = \frac{r_0}{1+r_0} \tag{20}$$

$$N = \frac{(1+2r_{45})(r_0+r_{90})}{2(1+r_0)r_{90}} \tag{21}$$

For planar anisotropy, if set $R_{11} = 1$, the other anisotropic yield stress ratios R_{22}, R_{33} and R_{12} are defined using the following relationships

$$R_{22} = \sqrt{\frac{r_{90}(r_0+1)}{r_0(r_{90}+1)}} \tag{22}$$

$$R_{33} = \sqrt{\frac{r_{90}(r_0+1)}{r_0+r_{90}}} \tag{23}$$

$$R_{12} = \sqrt{\frac{3(r_0+1)r_{90}}{(2r_{45}+1)(r_0+r_{90})}} \tag{24}$$

Based on the test results presented in Table 3 and using the above equations, Lankford coefficients and Hill's coefficients of DP600 steel are presented in Table 4.

Table 4: The Lankford coefficients and Hill's parameters of DP600 steel

r_0	r_{45}	r_{90}	R_{11}	R_{22}	R_{33}	R_{12}
1.0123	0.6487	0.9160	1	0.9748	0.9777	1.1172
F	G	H	N			
0.5492	0.4969	0.5031	1.2017			

Two yield surfaces predicted by Hill48 model and Von Mises criterion of the dual phase steel DP600 sheet are shown in figure 11.

The contour of residual stresses of two material rolling orientations $\theta = 0°$ and $\theta = 90°$ are presented in figure 12. With the material rolling orientation

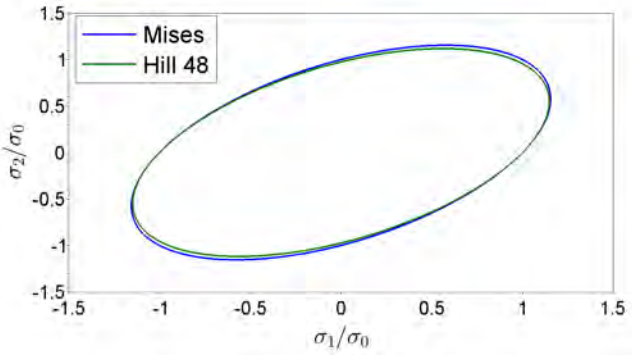

Figure 11: Yield surface predicted by Hill48 anisotropic model and Von Mises criterion

setting from longitudinal to transversal direction, the simulated distributions of residual stresses σ_{11} and σ_{22} turn over. The distributions of σ_{11} and σ_{22} with material rolling orientation $\theta = 0°$ correspond to the distribution of σ_{22} and σ_{11} with material rolling orientation $\theta = 90°$, respectively.

Residual stresses σ_{11} and σ_{22} along transversal path are simulated. Different material rolling orientations with $\theta = 0°$, $45°$ and $90°$ are applied in models. The simulation results are presented in figure 13. The material rolling orientation influence the magnitude of longitudinal and transversal residual stresses.

6. Model validation

To validate the obtained numerical results, specimen experiments have been realized using neutrons diffraction technique. A gauge volume of $1\times1\times5$ mm^3 was defined with the 5 mm aperture along the axis of the laser weld to improve intensity while has been possible (i.e. for transverse and longitudinal measurements only). For axial measurements, a sampling volume of $1 \times 1 \times 1$ mm^3 was used. The crystallographic texture of the base material was determined by neutron diffraction technique on the dedicated 4-circles diffractometer 6T1 at LLB (Hutchings et al. (2005)). From the {110}, {200} and {211} pole figures, using a $5° \times 5°$ grid, the Orientation Distribution Function (ODF) was calculated using LaboTex software (Pawlik and Ozga (1999)). The texture exhibits slight {hkl}<110> reinforcements, typical of a cold rolled ferritic steel, but the calculated texture index is rather low (1.6).

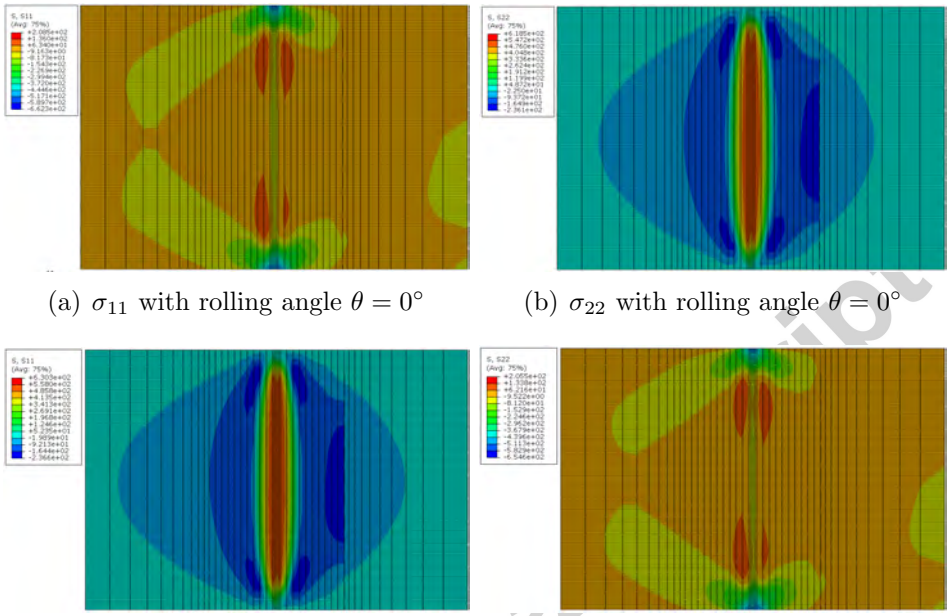

(a) σ_{11} with rolling angle $\theta = 0°$ (b) σ_{22} with rolling angle $\theta = 0°$

(c) σ_{11} with rolling angle $\theta = 90°$ (d) σ_{22} with rolling angle $\theta = 90°$

Figure 12: Contour of residual stresses with different material rolling orientations

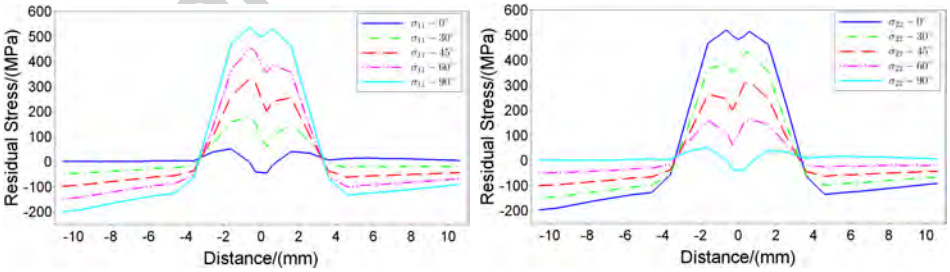

(a) Residual stresses of transversal direction (b) Residual stresses of longitudinal direction

Figure 13: Numerical welding residual stresses obtained from different rolling orientations

An elastic self-consistent calculation was performed considering the experimental texture to deduce the {110} dependent values for Young's modulus (E_{110}) and Poisson's ratio (ν_{110}): as a result, it appears that the elastic anisotropy should remain very low, with E_{110} ranging between 220 and 226 GPa, and ν_{110} between 0.31 and 0.35, depending on the considered direction. In a first approach, triaxial residual stresses were thus calculated from the measured strains applying the Hooke's law (equation 25) in the isotropic elasticity approximation:

$$\sigma_i = \frac{E_{110}}{1+\nu_{110}} \left[\varepsilon_i + \frac{\nu_{110}}{1-2\nu_{100}} \sum_j \varepsilon_j \right] \tag{25}$$

where i, j = axial, transverse and normal, and with the following values for Young's modulus $E_{110} = 220$ GPa and Poisson's ratio $\nu_{110} = 0.33$.

Since the characterized zones close to (Heat Affected Zone, HAZ) and within the weld (Fusion Zone, FZ) may have their microstructures more or less strongly affected by the welding process, chemical composition is likely to be heterogeneous depending on the distance from the center of the weld. One would thus commit an error if considering the base material as the reference material for unstrained lattice spacing. So, due to the low thickness of the studied plates, a zero normal stress state was assumed (i.e. a plane stress state), and theoretical reference lattice spacing and diffraction angles $2\theta_0$ could thus be calculated for each measurement point, applying the following formula (26), (Staron et al. (2004)):

$$2\theta_0 = 2 \cdot sin^{-1} \left(\frac{(1+\nu) \cdot sin\theta_{normal} \cdot sin\theta_{axial} \cdot sin\theta_{transverse}}{(1-\nu) \cdot sin\theta_{axial} \cdot sin\theta_{transverse} + \nu \cdot sin\theta_{normal} \cdot (sin\theta_{axial} + sin\theta_{transverse})} \right) \tag{26}$$

Considering the difficulty to obtain a reliable unstressed reference sample, the reference (unstressed) $d_{0,\{110\}}$ lattice spacing required for strain calculations was determined assuming a zero normal stress at 5 mm in the base metal from the center of the weld.

In figure 14, along the transversal path of weld, experimental and numerical results of residual stresses variations with the different material orientations are shown. The residual stresses of σ_{11} and σ_{22} are measured by Neutron Diffraction method along transversal path. The material is assigned a material rolling orientation that have 30° with transversal path. The simulation result shows a good accordance with experiment measurement.

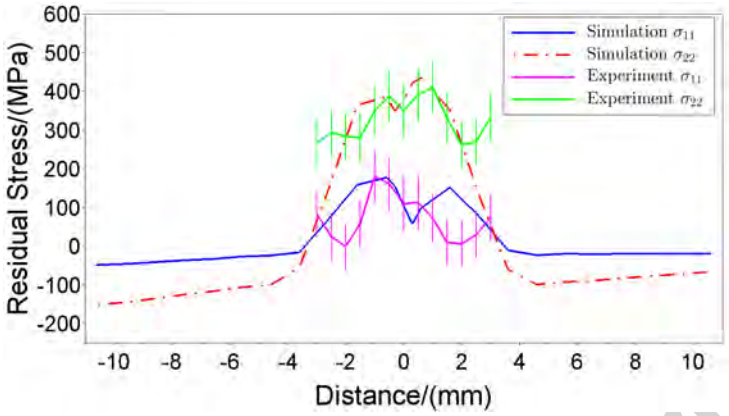

Figure 14: Comparison between the experimental and the numerical residual stresses

7. Conclusion

In this study, a sequential coupled thermo-mechanical FE model is built for a lap laser welding simulation to analyze the elasto-plastic behavior and the residual stress distributions of dual phase steel DP600 joints. Different mechanical constitutive material models describing the hardening behavior, the temperature sensitivity and the anisotropy of the plasticity of the DP600 steel are identified, analyzed and employed in the numerical simulation. By comparisons with neutrons diffraction measurements of residual stresses, the elastic-plastic thermo-mechanical FE model is proved to be useful in predicting the welding residual stresses. According to the simulation and experimental results, we can draw the following conclusions:

1. The flow stress of DP600 at room temperature is obtained from tensile test. Both the classical Ludwik hardening model and the Voce model can represent the obtained true stress-strain hardening behavior of DP600 only with a little mismatch. Improvements of these two classical laws can be obtained only if parameters identification is made in the plastic strain range [0, 0.05]. Thus, a synthesis model formulation based on Voce and Ludwik models has been proposed in order to precisely describe the observed behavior of DP600 steel. Comparative simulations are done for the identified Ludwik, Voce and synthesis hardening models. Similar residual stresses results are acquired by the three hardening models. The obtained results reveal that, as long as flow stresses obtained from formulations of different hardening

models are similar for a laser welding plastic strain range defined by $0< \varepsilon_p <0.05$, these ones have small influences on the corresponding numerical residual stresses .

2. Based on the experimental data corresponding to thermal mechanical properties of a high strength steel, the Johnson-Cook, Chen and Khan temperature sensitivity models together with a proposed model and a polynomial model are identified for DP600 material. Thermo-mechanical analyses show that the classical Johnson-Cook and the Khan temperature sensitivity terms are suitable to describe DP600 thermal softening behavior from room temperature to about 800K. For welding simulation that concerns high temperature up to about 1200K, the proposed and the Chen temperature sensitivity formulation show a better accordance with the obtained experimental data. The temperature sensitivity has a big influence on residual stresses simulation. Even the proposed temperature sensitivity formulation and the Chen model are nearly the same in description of temperature sensitivity, comparative simulations show some differences between the Chen model and the proposed one. Compared with the polynomial model (a best mathematical but not physical description of experimental temperature sensitivity), the proposed physical formulation results show better residual stresses of transversal direction while the Chen model results show better residual stresses of longitudinal direction.
3. Concerning the observed plane anisotropy of the DP600 steel, parameters of Hill-48 criterion are identified through several experiment tests. Simulations with different material rolling orientations of DP600 are assigned to material model. The material orientation of DP600 is found to have a big influence on simulation results of residual stresses σ_{11} and σ_{22}. The material orientation influence the magnitude of residual stresses σ_{11} and σ_{22}, increasing one while decreasing the other.
4. Experiment of laser welding with the same welding parameters of numerical model are conducted and residual stresses of the experiment sample are examined by a Neutron Diffraction technique. Based on the experiment measurements, increased residual tensile stresses are found at the weld area. Residual stresses of longitudinal direction σ_{22} are found to be higher than residual stresses of transversal direction σ_{11}. By comparison, the experimental results of residual stresses show good accordance with the numerical simulation results.

8. Acknowledge

The work was financially supported by China Scholarship Council, the Mecaprocess Team of INSA de Rennes and by CEA of Saclay for the experimental measurements.

Reference

Barlat, F., Aretz, H., Yoon, J., Karabin, M., Brem, J., Dick, R., 2005. Linear transfomation-based anisotropic yield functions. International Journal of Plasticity 21 (5), 1009–1039.

Barlat, F., Chung, K., 1993. Anisotropic potentials for plastically deforming metals. Modelling and Simulation in Materials Science and Engineering 1 (4), 403.

Bouaziz, O., Zurob, H., Huang, M., 2013. Driving force and logic of development of advanced high strength steels for automotive applications. steel research international 84 (10), 937–947.

Calcagnotto, M., Adachi, Y., Ponge, D., Raabe, D., 2011. Deformation and fracture mechanisms in fine-and ultrafine-grained ferrite/martensite dual-phase steels and the effect of aging. Acta Materialia 59 (2), 658–670.

Chen, D., Wang, Z., Jiang, X., Ai, S., Shih, C., 1989. The dependence of near-threshold fatigue crack growth on microstructure and environment in dual-phase steels. Materials Science and Engineering: A 108, 141–151.

Chen, J., Young, B., Uy, B., 2006. Behavior of high strength structural steel at elevated temperatures. Journal of structural engineering 132 (12), 1948–1954.

Chen, S., Huang, C., Wang, C., Duan, Z., 2008. Mechanical properties and constitutive relationships of 30crmnsia steel heated at high rate. Materials Science and Engineering: A 483-484, 105–108.

Davies, G., 2012. Materials for automobile bodies. Butterworth-Heinemann.

Farabi, N., Chen, D. L., Zhou, Y., 2011. Microstructure and mechanical properties of laser welded dissimilar dp600/dp980 dual-phase steel joints. Journal of Alloys and Compounds 509 (3), 982–989.

Fekete, J., Stibich, A., 2001. A comparison of the response of hsla and dual phase sheet in dynamic crush. In: International Body Engineering Conference & Exposition (IBEC), Detroit MI. Vol. 01. p. 3101.

Gavrus, A., 2012. Constitutive equation for description of metallic materials behavior during static and dynamic loadings taking into account important gradients of plastic deformation. Key Engineering Materials 504, 697–702.

Hazratinezhad, M., Mostafa Arab, N. B., Sufizadeh, A. R., Torkamany, M. J., 2012. Mechanical and metallurgical properties of pulsed neodymium-doped yttrium aluminum garnet laser welding of dual phase steels. Materials & Design 33, 83–87.

Hibbitt, Karlsson, Sorensen, 1997. ABAQUS: Theory Manual. Vol. 2. Hibbitt, Karlsson & Sorensen.

Hill, R., 1948. A theory of the yielding and plastic flow of anisotropic metals. In: Proceedings of the Royal Society of London A: Mathematical, Physical and Engineering Sciences. Vol. 193. The Royal Society, pp. 281–297.

Hutchings, M. T., Withers, P. J., Holden, T. M., Lorentzen, T., 2005. Introduction to the characterization of residual stress by neutron diffraction. CRC press.

Hutchison, M. M., 1963. The temperature dependence of the yield stress of polycrystalline iron. Philosophical Magazine 8 (85), 121–127.

John, G. R., Cook, W. H., 1983. A constitutive model and data for metals subjected to large strains, high strain rates and high temperatures. Proceedings of the 7th International Symposium on Ballistics 21, 541–547.

Khan, A. S., Sung Suh, Y., Kazmi, R., 2004. Quasi-static and dynamic loading responses and constitutive modeling of titanium alloys. International Journal of Plasticity 20 (12), 2233–2248.

Kuang, S., Kang, Y.-l., Yu, H., Liu, R.-d., 2009. Effect of continuous annealing parameters on the mechanical properties and microstructures of a cold rolled dual phase steel. International Journal of Minerals, Metallurgy and Materials 16 (2), 159–164.

Ludwik, P., 1909. Element der technologischen. Mechanik, 32.

Marya, M., Gayden, X., 2005. Development of requirements for resistance spot welding dual-phase (dp600) steels part 1—the causes of interfacial fracture. Welding Journal 84 (11), 172–182.

Ohashi, K., Utsunomiya, H., Matsumoto, R., 2012. Evaluation of r-value of steels using vickers hardness test. Journal of Physics: Conference Series 379, 012045.

Ozturk, F., Toros, S., Kilic, S., 2014. Effects of anisotropic yield functions on prediction of forming limit diagrams of dp600 advanced high strength steel. 11th International Conference on Technology of Plasticity, ICTP 2014, 19-24 October 2014, Nagoya Congress Center, Nagoya, Japan 81, 760–765.

Padmanabhan, R., Baptista, A., Oliveira, M., Menezes, L., 2007. Effect of anisotropy on the deep-drawing of mild steel and dual-phase steel tailor-welded blanks. Journal of Materials Processing Technology 184 (1-3), 288–293.

Pawlik, K., Ozga, P., 1999. Labotex: the texture analysis software. Göttinger Arbeiten zur Geologie und Paläontologie, SB4.

Rabahallah, M., Balan, T., Bouvier, S., Bacroix, B., Barlat, F., Chung, K., Teodosiu, C., 2009. Parameter identification of advanced plastic strain rate potentials and impact on plastic anisotropy prediction. International Journal of Plasticity 25 (3), 491–512.

Samantaray, D., Mandal, S., Bhaduri, A., 2010. Constitutive analysis to predict high-temperature flow stress in modified 9cr-1mo (p91) steel. Materials & Design 31 (2), 981–984.

Seang, C., David-Kouadri, A., Ragneau, E., 2013. Nd: Yag laser welding of sheet metal assembly: Transformation induced volume strain affect on elastoplastic model. Physics Procedia 41, 448–459.

Staron, P., Kocak, M., Williams, S., Wescott, A., 2004. Residual stress in friction stir-welded al sheets. Physica B: Condensed Matter 350 (1), E491–E493.

Voce, E., 1955. A practical strain-hardening function. Metallurgia 51 (307), 219–226.

Xia, M., Biro, E., Tian, Z., Zhou, Y. N., 2008. Effects of heat input and martensite on haz softening in laser welding of dual phase steels. ISIJ International 48 (6), 809–814.